

# Dynamic Soil Pressures on Embedded Retaining Walls: Predictive Capacity Under Varying Loading Frequencies

B. Mendez<sup>1</sup>, D. Rivera<sup>2</sup>

## ABSTRACT

Results obtained with traditional limit equilibrium methods for dynamic pressures on embedded walls are analyzed and compared to numerical simulations of a retaining wall subjected to harmonic input motions for different frequencies. Results are compared in terms of dynamic pressure distribution and total dynamic force. A model built in FLAC for the analysis considers non-linear soil properties, stress-dependent soil modulus and interface elements to model soil-wall interaction. Hysteretic damping is accounted for during dynamic loading. Harmonic waves of different frequencies are used as input motion, as well as an actual earthquake record of broad frequency content to compare to analytical results. Preliminary analyses have shown that there is a noticeable difference in the predictive capacity of limit equilibrium methods for computing dynamic pressures when considering harmonic or earthquake loading. It is expected that results help to make a more insightful use of simplified methods.

## Introduction

A numerical experiment is presented in this paper that shows how conventional limit equilibrium methods (*e.g.*, Mononobe-Okabe) perform under different dynamic loading conditions. Due to its wide spread use in engineering practice, focus will be made on the Mononobe-Okabe method (M-O). The M-O is used to compare its results to those computed numerically for a case study of an embedded retaining wall subjected both to a harmonic and earthquake loading. The comparison is made in terms of dynamic soil pressure distribution and total dynamic force. The numerical analysis is performed using FLAC3D 4.00 for a two-dimensional model.

## Numerical Model

The case study considered for the analyses is depicted in Figure 1. The model consists of a 5 m depth excavation retained by an embedded cantilevered wall. The excavation is performed in 1 m depth stages in a dry layered coarse-grained soil with the properties and constitutive material models presented in Figure 1 (a). The selection of these properties and constitutive models was made by calibrating a numerical triaxial test performed in FLAC3D with laboratory results obtained with triaxial tests on homothetic configurations, executed by De La Hoz (2007) for a coarse-grained soil. This calibration is presented in the next section of this paper.

The retaining wall is modeled as a double-sided liner element, thus having soil-wall interaction on both sides of the wall. The wall was first installed into the soil, and then the

---

<sup>1</sup>Ph.D., B. Mendez, Rizzo Associates, Santiago, Chile, [bogart.mendez@rizzoassoc.cl](mailto:bogart.mendez@rizzoassoc.cl)

<sup>2</sup>M.Sc., D. Rivera, Rizzo Associates, Pittsburgh, USA, [diego.rivera@rizzoassoc.com](mailto:diego.rivera@rizzoassoc.com)

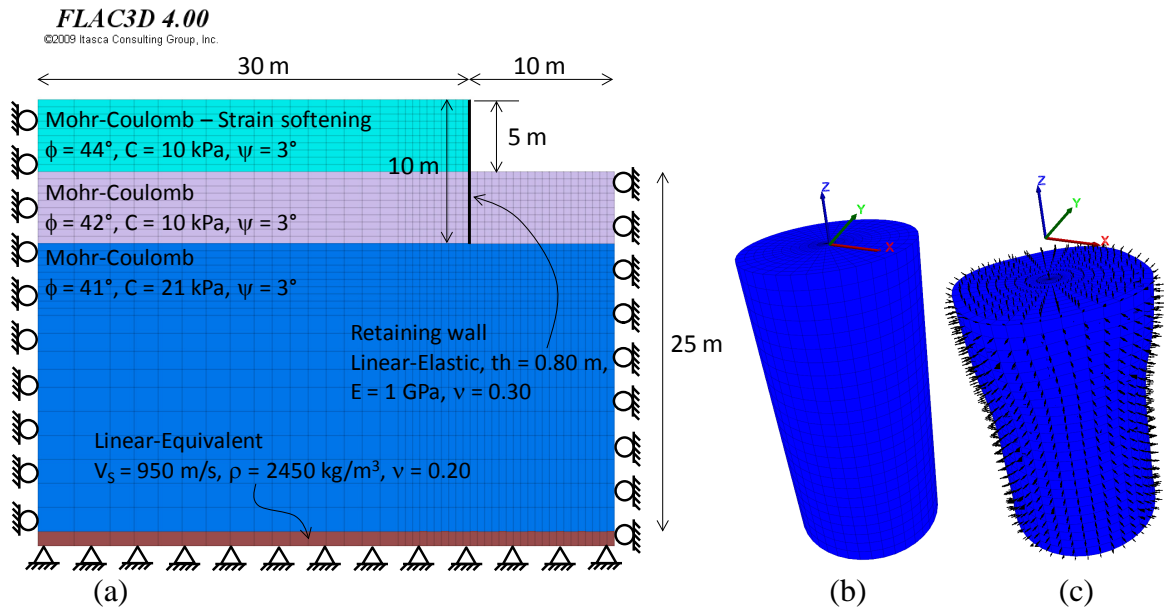


Figure 1. (a) Geometry of case study analyzed, (b) original and (c) sheared sample geometries in the numerical triaxial test executed

side in front of the wall was excavated in five stages. The wall-soil contact has an elastic-plastic behavior with a Mohr-Coulomb failure criterion. The interface friction angle is  $30^\circ$  and a cohesion of 5 kPa is considered. The value of Normal and shear coupling stiffnesses were assigned based on the apparent stiffness of the soil elements on both sides of the wall. The soil element sizes close to the wall are 0.50 m and they gradually increase up to 1.70 m until the bottom of the model. The embedded portion of the retaining wall has the same length of its cantilevered portion. This proportion is relevant in the development of dynamic soil pressures (Francesco *et al.*, 2010), but analyzing its effect is out of the scope of this research.

### Material Properties and Constitutive Model for Static Loads

A Mohr-Coulomb material model is used to simulate the behavior of coarse-grained soils. As the case study model considers a layered deposit, the first soil layer was modeled with a strain-softening material to degrade soil cohesion as a function of plastic strain. Friction angle and cohesion properties were calibrated as a function of confining stress using experimental results obtained by De La Hoz (2007) with homothetic strain-controlled triaxial tests executed in coarse-grained soils.

The calibration was performed by simulating De La Hoz (*op. cit.*) experiments in FLAC3D, executing a numerical triaxial test. A view of the numerical 3D sample is presented in Figure 1 (b) and (c). The soil Young modulus is stress-dependant during the test. The modulus variation given by De La Hoz can be expressed in terms of as  $E = 136080(\sigma_{oct})^{0.48}$ , where  $E$  and  $\sigma_{oct}$  are given in Pascals.

The numerical samples have dimensions of 15x30 cm and were tested under confining stresses of 100, 200 and 400 kPa. Results of the simulations are presented in Figure 2 in terms of stress-strain curves. It is observed from Figure 2 that Mohr-Coulomb model reproduces the overall behavior of the granular material. The use of more complex soil models could have a closer approximation of the material behavior. However, a detailed

calibration with such models is out of the scope of this paper. It is considered that the behavior achieved with the Mohr-Coulomb model is adequate for the purpose of this research. The model parameters used during the simulations that produced the curves of Figure 2 are presented in Table 1. Soil cohesion during the 100 kPa triaxial simulation varied with plastic shear strain. The variation was obtained from experimental results presented in the De La Hoz document (2007).

Table 1. Material properties used in the numerical triaxial tests

Test	$\phi$	C, kPa	$\psi$	$\rho$ , kg/m <sup>3</sup>	$\nu$
100 kPa	44°	Varies	3	2115	0.20
200 kPa	42°	10	3	2116	0.20
400 Kpa	41°	21	3	2161	0.20

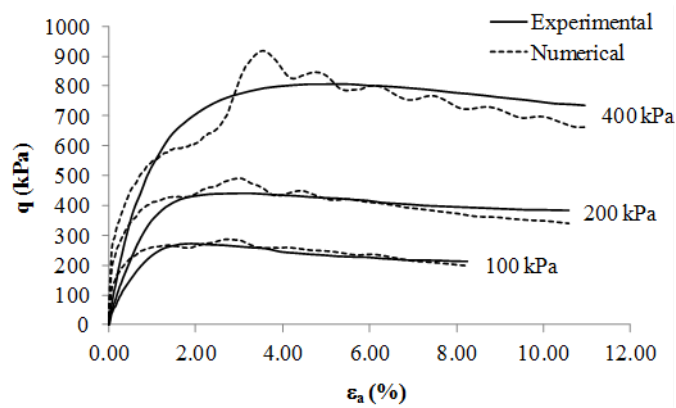


Figure 2. Experimental vs numerical results from triaxial tests by De La Hoz (2007)

### Dynamic Material Properties

Initial shear wave velocity,  $V_s$ , and small-strain shear modulus,  $G_0$ , profiles adopted for the coarse-grained soil are presented in Figure 3 (a) and (b). These properties are consistent with a good quality gravelly deposit, with an average shear wave velocity of 664 m/s in the upper 30 m ( $V_{s30}$ ). The rock layer is set at 30 m depth for the case study analyzed, and the material density is 2200 and 2450 kg/m<sup>3</sup> for the gravel and rock, respectively.

Shear modulus degradation and damping curves adopted for the dynamic analyses are presented in Figure 3 (c) and (d), respectively. To account for the effect of confinement in dynamic material properties, several curves are proposed for different depths. As a reference, the curves shown in Figure 3 show the limits of Seed *et al.* (1986) for granular materials. Damping is limited to a maximum value of 15 % for large shear strains out of the applicability range of the linear-equivalent method. However, it was verified that for linear-equivalent analyses, the maximum shear strains were within the applicability of this method.

Degradation curves were used in two ways in this research: (1) in SHAKE analysis to validate FLAC3D free-field dynamic response, and (2) to have hysteretic damping in the elastic portion of the non-linear FLAC3D analyses. In these analyses, once yielding is

reached, damping is achieved “naturally” due to energy dissipation in the plastic range of the soil constitutive model.

### Free Field Dynamic Response

The free field dynamic response obtained with non-linear FLAC3D analyses was verified using SHAKE equivalent-linear analyses. To this end, a time series registered on rock during the 2010 Maule Earthquake in Chile was used as the input motion for both FLAC3D and SHAKE models. The input motion has a PGA = 0.30 g and a maximum frequency of 25 Hz with a duration of 72 seconds. The element sizes in the FLAC3D model are compatible with the frequency content of the input motion (Kuhlemeyer and Lysmer, 1973), resulting in a maximum element size of 26 m for a 25 Hz frequency considering 8 elements for wavelength. The wavelength used for this element size computation is  $V_{S30}$  shown in Figure 3 (a). This element size is much larger than the actual sizes used (up to 1.70 m) in the model, thus ensuring an adequate frequency transmission across the model. Seismic-induced maximum shear strains were within the applicability range of the linear-equivalent method. An effective shear strain of 65 % is considered for both SHAKE and FLAC3D analyses. As shown in Figure 4 (a), (b) and (c), results are compared in terms of maximum shear strains, response and Fourier spectra, respectively. It is observed in these figures that free field computed with both codes is practically identical, thus validating FLAC3D dynamic response analyses.

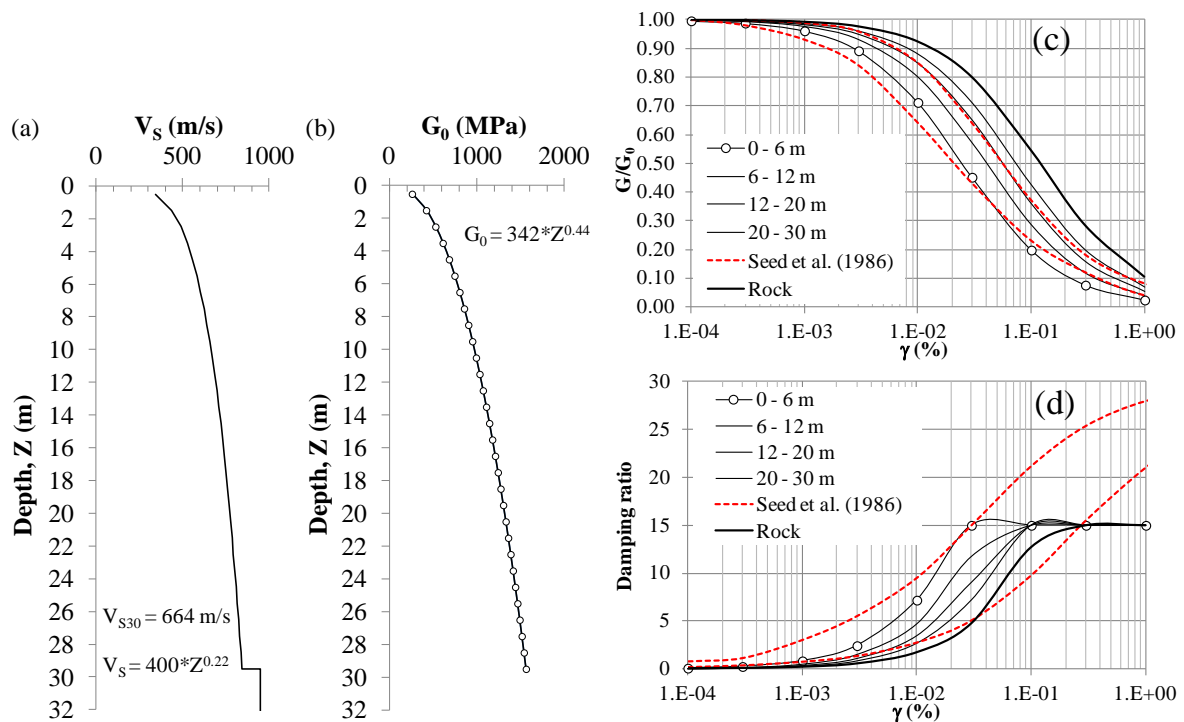


Figure 3. Initial variation of  $V_s$  (a) and  $G_0$  (b) for the soil profile, shear modulus degradation (c) and damping ratio (d) curves

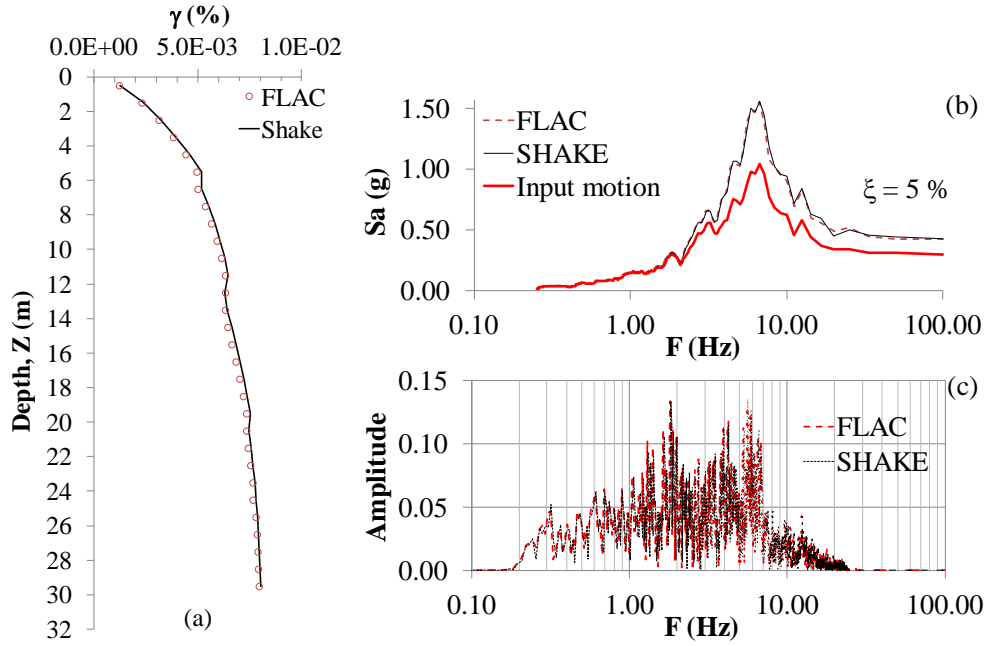


Figure 4. Comparison of (a) max shear strains, (b) response and (c) Fourier spectra

### Results for Dynamic Soil Pressures under Harmonic Loading

After achieving static equilibrium in the excavation, harmonic loads were applied to the model. The set of harmonic signals used for the analyses is shown in Table 2. All signals have the same acceleration amplitude,  $\ddot{U}_0$ , equal to 0.30 g, which corresponds to the PGA of the earthquake record used for calibrating free field response. This time history is also used for the analysis of seismic load in the next section of this paper. The corresponding velocity,  $V_0$ , and displacement,  $D_0$ , of harmonic signals are also presented in Table 2. The frequency of each harmonic signal,  $F$ , was selected based on the site initial frequency,  $F_{\text{site}} = 5.53$  Hz (one-dimensional response frequency, *i.e.*,  $V_{S30}/4H$ ), to have a broad range of frequency ratios ( $F/F_{\text{site}}$  values). All signals have the same duration,  $T_d = 1$  second, which was chosen as the closest round duration value approximately matching the Arias intensity of the earthquake record used for calibrating free field response.

Numerical dynamic soil pressure distributions were computed at different time instants for each harmonic load. Each signal was applied after achieving the static stress distribution. Computed stresses are total stresses, as they include both static and dynamic components. Total dynamic force was computed by integrating the dynamic stress distribution at the end of load duration. For the analytical calculations with M-O, two seismic coefficients were considered:  $k_h = \text{PGA}/2$  and  $k_h = \text{PGA}$ . These values are selected as they are commonly used in engineering practice. Results in terms of dynamic soil pressure distributions, normalized total force and displacements, are presented in Figure 5 (a), (b) and (c), respectively. The horizontal dynamic soil stresses,  $\sigma_h$ , presented in Figure 5 (a) are the average values computed during harmonic loading duration. Static soil pressures are very low in the upper part of the wall due to soil cohesion. It is noted from this figure that, for frequency ratios lower than three, total stresses during dynamic loading can be much higher than those computed with M-O for the lower half of the wall height. On the other hand, when compared to low frequency ratios, high frequency ratios (above 3) produce larger pressures on the upper half of the wall (above 2 m depth, approximately). It is interesting to note that these

differences in wall response for several frequencies develop above and below a certain point (inflection point), located about 2 m depth for the case analyzed, which approximately coincides with the so-called ‘active pile length’, beyond which a head-loaded pile behaves as an infinitely long beam (Nikolau *et al.*, 2001). As the case of a laterally-loaded pile, the embedded retaining wall only mobilizes a relatively short portion of its length when seismically loaded, as will be further shown for the case of earthquake loading. For the case analyzed in this paper, the theoretical active length computed varies around 2.1 – 2.5 m, which is about the depth observed of the inflection point. This fact evidences the effects of soil-wall interaction and possibly non-linear effects. Consider wall displacements shown in Figure 5 (c), which correspond to the top of the wall. It is noted in this figure that displacements increase for lower frequency ratios, and diminish for high frequency ratios. This complies well with the pressure distributions shown in Figure 5 (a), where lower values develop for low frequency ratios in the upper part of the retaining wall (from 2 m and above), while the lower zone of the wall shows the opposite behavior, *i.e.*, seismic pressure increases with increase of the frequency ratio. This supports the idea of non-linearity effects on the dynamic behavior of the soil-wall system. On the other hand, it is observed that for all frequency ratios, pressures during dynamic loading are lower than the static value at the bottom of the wall (below 4.25 m), where passive soil pressures develop.

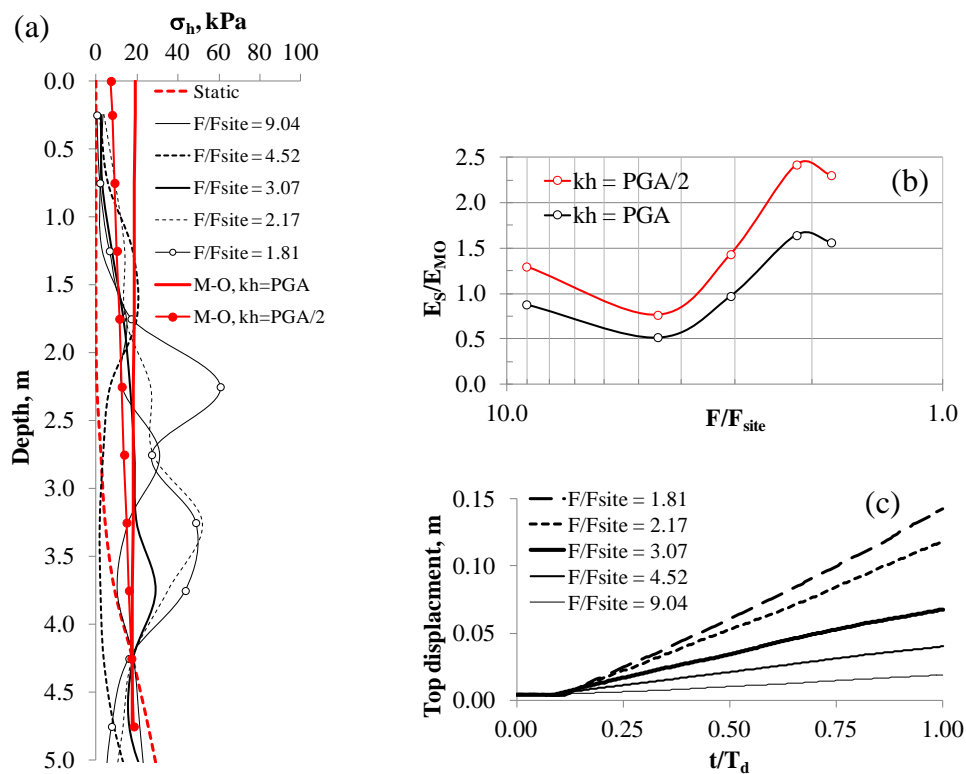


Figure 5. (a) Dynamic soil pressure distributions, normalized force (b) and displacements (c)

When looking to the total force exerted on the wall, Figure 5 (b) presents the total average soil force on the wall (*i.e.*, static + dynamic) at the end of dynamic loading,  $E_S$ , normalized with the total force computed using M-O with  $k_h = \text{PGA}$  and  $k_h = \text{PGA}/2$ ,  $E_{MO}$ . It is noted that M-O method with  $k_h = \text{PGA}$  produces a conservative result for frequency ratios above three. On the other hand, M-O method with  $k_h = \text{PGA}/2$  computes lower total soil pressures for all frequency ratios, except for  $F/F_{site} = 4.52$ . The M-O method produces lower pressures for frequency ratios two and below, regardless of the seismic coefficient. This is

consistent with the results of Francesco *et al.* (2010), who found that for frequency ratios between 1 and 2 M-O method is not capable of reproducing dynamic amplification.

Table 2. Harmonic loads considered in the analyses

Signal	F (Hz)	F/F <sub>site</sub>	$\ddot{U}_0$ (g)	V <sub>0</sub> (m/s)	D <sub>0</sub> (m)	T <sub>d</sub> (sec)
1	50	9.04	0.30	0.0094	2.98E-5	1.00
2	25	4.52	0.30	0.0187	1.19E-4	1.00
3	17	3.07	0.30	0.0276	2.58E-4	1.00
4	12	2.17	0.30	0.0390	5.18E-4	1.00
5	10	1.81	0.30	0.0468	7.45E-4	1.00

### Results for Dynamic Soil Pressures under Earthquake Loading

Time history used in the analyses is the same used for the free field model calibration shown earlier in this paper. The record corresponds to a rock record obtained during the Maule Earthquake in Chile (Boroschek *et al.*, 2010). Results are presented in terms of response spectra, soil displacements on top of the failure wedge, soil pressure distributions and total exerted force on the wall. Response spectra in Figure 6 (b) at  $Z = 0$  m correspond to the location at top of the failure wedge, and the spectra at  $Z = -5$  m correspond to the location at the bottom of the excavation. It is clear how the spectrum at  $Z = 0$  m has lower spectral acceleration than the other locations, due to the non-linear soil effect. On the other hand, the free field spectrum is very similar to that computed with SHAKE (*i.e.*, linear equivalent method), thus indicating that free field response does not show significant non-linear effects.

In terms of soil pressure distribution, it is observed from Figure 6 (a) that M-O pressures are generally similar to those computed numerically, but with some local variations. Numerical pressure distributions at time instant of peak ground displacement (46 seg) and at the end of excitation (72 seg) are plotted in Figure 6 (a) for comparison. It is observed that soil pressures decreased after time instant of 46 s, where displacements increased during seismic loading, thus suggesting soil yielding effects. Also, as in the case of harmonic loading, soil pressures during earthquake loading are lower than static pressures at the lower portion of the wall, at about 4 m and below, where passive soil pressures develop. This conforms well to the level of displacement in the wall, where the lower portion of the retaining wall shows smaller displacement (relative to its base), which increases seismic pressures, while the upper zone develops larger displacements thus decreasing soil pressures. Similar results have been observed by other authors (*e.g.*, Gazetas *et al.*, 2004), where for the case of flexible retaining walls, computed seismic pressures are lower than those computed by the M-O method (considering  $kh = 0.75 \cdot \text{PGA}$ ), especially for the upper part of the retaining elements.

When compared to results obtained for harmonic loading, Figure 6 (a) shows that earthquake loading (broad frequency content) excites the wall along its full depth and higher stresses develop in the upper part of the wall (about 2.5 m and above) with respect to its lower portion, either at peak ground displacement (46 s) or at the end of loading (72 s). It is interesting to note that seismic pressures are similar in the lower portion of the wall (about 2.5 m and below) for both time instants, and show differences in the upper portion. This

approximately coincides with the active length of the wall (similar to a pile, see Nikolau *et al.*, 2001). As stated before in this paper, a similar result was observed for harmonic loading. This is interesting and might suggest the developing of an effective soil failure wedge for this type of walls, instead of using a seismic-intensity – dependent wedge with the M-O. This approach of a fixed wedge has recently been proposed by other authors (Tsai and Newman, 2014), thus it would be interesting to explore this possibility in further studies.

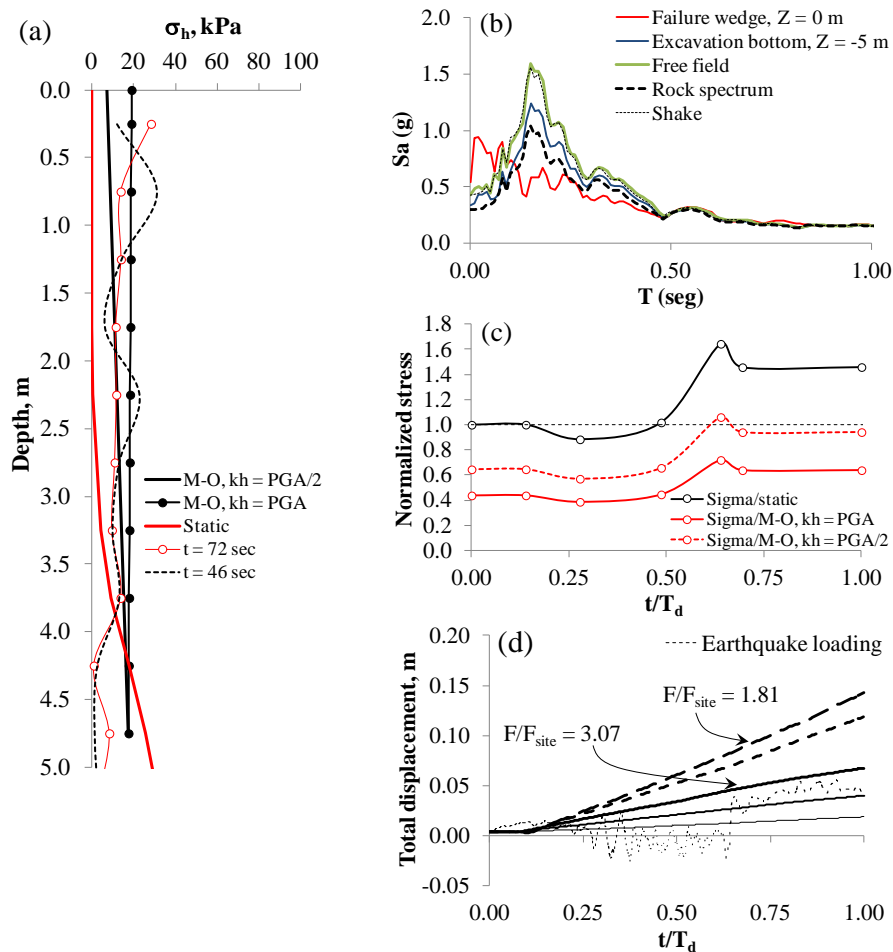


Figure 6. (a) Dynamic soil pressure distributions, (b) response spectra, normalized force (c) and displacements on top of the wall (d)

For the total force exerted on the wall, it is noted in Figure 6 (c) that the M-O method with  $k_h = \text{PGA}/2$  (where  $\text{PGA} = 0.30$  g) satisfactorily matches the total force computed numerically at the end of earthquake loading. On the other hand, as opposed for the harmonic loading case, where the M-O method with  $k_h = \text{PGA}$  showed closer results to numerical calculations, for the case of earthquake loading the use of  $k_h = \text{PGA}$  seems to be over conservative (*e.g.*, Watanabe *et al.*, 2011; Gazetas *et al.*, 2004).

## Conclusions

For the case analyzed, the harmonic load case results showed that M-O method tends to underestimate total soil force exerted on the embedded wall, while for the case of earthquake loading M-O calculations were closer to numerical values. In terms of pressure distribution,



M-O can under-predict its value both for harmonic and earthquake loading. For the earthquake loading this varies during loading application. It was observed for both loading cases that an inflection point developed in the wall, which divided different behaviors observed above and below this point: for harmonic loading, dynamic soil pressures increased with loading frequency above this point, and the opposite behavior was observed below it. This evidences a strong influence of loading frequency, which cannot be taken into account with M-O method. For the case of earthquake loading, below this inflection point, it was observed that seismic soil pressures were very similar during loading duration, and differed above it. This behavior is not captured by the M-O method either, and suggests the developing of an effective soil failure wedge which should be investigated in future analyses.

## References

- Boroschek R, Soto P, Leon R (2010). University of Chile: <http://terremotos.ing.uchile.cl/2007>
- De la Hoz, K (2007). *Estimation of shear strength parameters in coarse granular soils*. U. of Chile, M.Sc. thesis.
- Francesco L, Foti S, Lancellotta R, Mylonakes G. Dynamic response of cantilever retaining walls considering soil non-linearity. *5th International Conference on Recent Advances in Geotechnical Earthquake Engineering and Soil Dynamics*, San Diego, California, 2010
- Gazetas, G. Psarropoulos, P.N.; Anastasopoulos, I.; Gerolymos, N. (2004). Seismic behavior of flexible retaining systems subjected to short-duration moderately strong excitation, *Soil Dynamics and Earthquake Engineering*, **24**[7]: 537-550.
- Kuhlemeyer R La nd Lysmer J (1973). Finite element method accuracy for wave propagation problems. *Journal of the Soil Mechanics and Foundations Division*, ASCE; **99**(5): 421-427
- Nikolaou S., Mylonakis G., Gazetas G., Tazoh T. (2001), "Kinematic pile bending during earthquakes: analysis and field measurements", *Géotechnique*, **51**(5), pp. 425-40.
- Seed H, Wong T, Idriss I M, Tokimatsu K (1986). Moduli and damping factors for dynamic analyses of cohesionless soils. *Journal of Geotechnical Engineering—ASCE* ;**112**(11) : 1016–32.
- Tsai CC, Newman EJ (2014). Wedge size issues on calculating seismically induced lateral earth pressure for retaining structures – an overview and a new simple approach. *Soils and Foundations*; **9**(2): 45-53
- Watanabe K, Koseki J, Tateyama M (2011). Seismic earth pressure exerted on retaining walls under a large seismic load. *Soils and Foundations*; **51**(3): 379-394